American Mineralogist, Volume 105, pages 1088–1098, 2020

Crystal-chemistry of sulfates from the Apuan Alps (Tuscany, Italy). VI. Tl-bearing alum-(K) and voltaite from the Fornovolasco mining complex

Cristian Biagioni[1,*], Daniela Mauro[1], Marco Pasero[1], Elena Bonaccorsi[1], Giovanni Orazio Lepore[2,†], Federica Zaccarini[3], and Henrik Skogby[4]

[1]Dipartimento di Scienze della Terra, Università di Pisa, Via S. Maria 53, I-56126 Pisa, Italy
[2]CNR-IOM-OGG c/o ESRF, 71 Avenue des Martyrs CS 40220 F-38043 Grenoble Cedex 9, Grenoble, France
[3]Department of Applied Geological Sciences and Geophysics, University of Leoben, Peter Tunner Str. 5, A-8700 Leoben, Austria
[4]Department of Geosciences, Swedish Museum of Natural History, Box 50007, SE-10405 Stockholm, Sweden

Abstract

Thallium-bearing samples of alum-(K) and voltaite from the Fornovolasco mining complex (Apuan Alps, Tuscany, Italy) have been characterized through X-ray diffraction, chemical analyses, micro-Raman, infrared (FTIR), Mössbauer, and X-ray absorption spectroscopy (XAS). Alum-(K) occurs as anhedral colorless grains or rarely as octahedral crystals, up to 5 mm. Electron-microprobe analysis points to the chemical formula $(K_{0.74}Tl_{0.10})_{\Sigma 0.84}(Al_{0.84}Fe_{0.14})_{\Sigma 0.98}S_{2.03}O_8 \cdot 12H_2O$. The occurrence of minor NH_4^+ was detected through FTIR spectroscopy. Its unit-cell parameter is a = 12.2030(2) Å, V = 1817.19(9) Å^3, space group $Pa\bar{3}$. Its crystal structure has been refined down to R_1 = 0.0351 for 648 reflections with $F_o > 4\sigma(F_o)$ and 61 refined parameters. The crystal structure refinement agrees with the partial substitution of K by 12 mol% Tl. This substitution is confirmed by XAS data, showing the presence of Tl^+ having a first coordination shell mainly formed by 6 O atoms at 2.84(2) Å. Voltaite occurs as dark green cubic crystals, up to 1 mm in size. Voltaite is chemically zoned, with distinct domains having chemical formula $(K_{1.94}Tl_{0.28})_{\Sigma 2.22}(Fe^{2+}_{3.57}Mg_{0.94}Mn_{0.55})_{\Sigma 5.06}Fe^{3+}_{3.06}Al_{0.98}S_{11.92}O_{48} \cdot 18H_2O$ and $(K_{2.04}Tl_{0.32})_{\Sigma 2.36}(Fe^{2+}_{3.83}Mg_{0.91}Mn_{0.29})_{\Sigma 5.03}Fe^{3+}_{3.05}Al_{0.97}S_{11.92}O_{48} \cdot 18H_2O$, respectively. Infrared spectroscopy confirmed the occurrence of minor NH_4^+ also in voltaite. Its unit-cell parameter is a = 27.2635 Å, V = 20265(4) Å^3, space group $Fd\bar{3}c$. The crystal structure was refined down to R_1 = 0.0434 for 817 reflections with $F_o > 4\sigma(F_o)$ and 87 refined parameters. The partial replacement of K by Tl is confirmed by the structural refinement. XAS spectroscopy showed that Tl^+ is bonded to six O atoms, at 2.89(2) Å. The multi-technique characterization of thallium-bearing alum-(K) and voltaite improves our understanding of the role of K-bearing sulfates in immobilizing Tl in acid mine drainage systems, temporarily avoiding its dispersion in the environment.

Keywords: Alum-(K), voltaite, thallium, XAS, crystal structure, Fornovolasco, Apuan Alps, Tuscany, Italy

Introduction

Thallium (Z = 81) is a toxic heavy element, classified as one of the 13 priority metal pollutants (Keith and Telliard 1979) and having an average concentration in the upper continental crust of 0.75 μg/g (Wedepohl 1995). Thallium occurs in two different oxidation states, i.e., Tl^+ and Tl^{3+}. Monovalent Tl has both a lithophile and chalcophile geochemical behavior, being enriched in K-bearing minerals as well as in several chalcogenides. In particular, the ionic radius of Tl^+ is close to that of K^+ and Rb^+ (e.g., Shannon 1976). Indeed, the only three secondary Tl^+-minerals known up to now as products of sulfide weathering, i.e., dorallcharite, $TlFe^{3+}_3(SO_4)_2(OH)_6$ (Balić-Žunić et al. 1994), lanmuchangite, $TlAl(SO_4)_2 \cdot 12H_2O$ (Chen and Wang 2001), and thalliumpharmacosiderite, $TlFe_4(AsO_4)_3(OH)_4 \cdot 4H_2O$ (Rumsey et al. 2014), are the counterparts of the K-minerals jarosite, alum-(K), and pharmacosiderite, respectively. Götz et al. (1968) described "monsmedite" as a new K-Tl^{3+} sulfate, with approximate chemical formula $Tl_2O_3 \cdot K_2O \cdot 8SO_3 \cdot 15H_2O$. This species was later discredited by the then IMA-CNMMN (Grice and Ferraris 2003), and the reinvestigation of several samples and co-type material by some authors (e.g., Johan et al. 2009; Kovács-Pálffy et al. 2011) showed that "monsmedite" is simply Tl-bearing voltaite.

The identification of the thallium-rich nature of the pyrite ore deposits of the southern Apuan Alps (northern Tuscany, Italy), with up to more than 4000 μg/g Tl (Biagioni et al. 2013; George et al. 2018), gave rise to a series of mineralogical and geochemical studies that led to the description of the dispersion of thallium in the environment (D'Orazio et al. 2017; Biagioni et al. 2017; Perotti et al. 2018; Ghezzi et al. 2019). Sulfate assemblages play a major role in the control of the release of heavy metals in the environment, and their mineralogical characterization is being currently undertaken. Our attention is mainly focused on the assemblages found in the Fornovolasco mining complex, where

* E-mail: cristian.biagioni@unipi.it
† Orcid 0000-0002-7984-3099.

the highest Tl contents in pyrite ores have been reported (e.g., D'Orazio et al. 2017). Since the first description of volaschioite (Biagioni et al. 2011), more than 15 different sulfate species have been identified in this locality. Among them, the two K-sulfates alum-(K) and voltaite are particularly interesting, owing to their significant Tl content.

The aim of this paper is the full characterization of Tl-bearing alum-(K) and voltaite from Fornovolasco (Apuan Alps, Tuscany, Italy), providing data for assessing the role played by K-sulfates in the transient sequestration of thallium in the acid mine drainage systems. Therefore, these minerals have been characterized through single-crystal X-ray diffraction, electron microprobe analysis, and some spectroscopic techniques, i.e., micro-Raman, infrared, Mössbauer, and X-ray absorption spectroscopy (XAS).

Experimental methods

The studied specimens (Fig. 1) were collected in the 740 m level of the pyrite-iron oxide mine of Fornovolasco (Apuan Alps, Tuscany, Italy). Alum-(K) occurs as crude colorless octahedral crystals, up to 5 mm in size, associated with römerite, copiapite, and minor voltaite. Voltaite occurs as cubic crystals, with minor octahedral and rhombic dodecahedral faces, dark green in color, up to 1 mm, usually associated with halotrichite and römerite.

Quantitative chemical data were collected on these samples through a Superprobe JEOL JXA 8200 electron microprobe at the "Eugen F. Stumpfl" laboratory (Leoben University, Austria). The following analytical conditions were used: WDS mode, accelerating voltage 10 kV (15 kV for thallium analysis), beam current 10 nA. Beam size was set to 20 μm to minimize sample damage. Standards were (element, emission line): magnetite (Fe*Kα*), TlBr (Tl*Mα*), sanidine (K*Kα*), albite (Al*Kα*), olivine (Mg*Kα*), rhodonite (Mn*Kα*), and baryte (S*Kα*). The ZAF routine was applied for the correction of the recorded raw data. Counting times were 15 s for peak and 5 s for left and right backgrounds. Several difficulties occurred during the preparation and the analysis of sulfate samples, mainly related to their instability under the electron beam and the high vacuum, and for the burst of the fluid inclusions entrapped in the analyzed grains, able to destroy the carbon coating and the polished surface. These inconveniences were particularly critical during the analysis of alum-(K). Indeed, the electron beam created some pits, several micrometers across, on the sample, owing to the strong dehydration and the burst of fluid inclusions. Consequently, only one spot analysis, normalized to 100 wt%, was obtained on alum-(K). Backscattered electron (BSE) images of voltaite showed the occurrence of a strong chemical zonation (see below), studied through X-ray maps whose collection was carried out on the basis of the same analytical conditions used for electron microprobe analyses. Chemical data are given in Table 1.

The ^{57}Fe Mössbauer spectrum of voltaite was collected at room temperature in transmission mode using a ^{57}Co (in Rh matrix) point source with a nominal activity of 0.40 GBq at the Swedish Museum of Natural History, Stockholm, Sweden. Fifteen crystals were mounted on a sticky tape and were positioned closely in front of the point-source. The Mössbauer spectrum was acquired over the velocity range ±4 mm/s and was calibrated against α-Fe foil. The spectrum was fitted using the program MossA (Prescher et al. 2012).

Micro-Raman spectra of alum-(K) and voltaite were collected on unpolished samples in nearly backscattered geometry using a Jobin-Yvon Horiba XploRA Plus apparatus, equipped with a motorized *x*-*y* stage and an Olympus BX41 microscope with a 10× objective lens. The Raman spectra were excited using a 532 nm line of a solid-state laser attenuated to 10% (2.5 mW) to minimize sample damage. The minimum lateral and depth resolution was set to a few micrometers. The system was calibrated using the 520.6 cm^{-1} Raman band of silicon before each experimental session. Spectrum was collected through multiple acquisitions with single counting times of 120 and 60 s for alum-(K) and voltaite, respectively. Backscattered radiation was analyzed with a 1200 gr/mm grating monochromator. Peak deconvolution was performed using Fityk (Wojdyr 2010).

Unpolarized FTIR absorption spectra of alum-(K) and voltaite were measured on gently powdered sample material mixed with KCl and pressed to a pellet. A Bruker Vertex spectrometer equipped with a Globar source, a KBr beam-splitter, an MCT detector, and a Hyperion 2000 microscope was used to acquire spectra in the wavenumber range 6000–600 cm^{-1} with a resolution of 4 cm^{-1}.

X-ray absorption spectroscopy (XAS) measurements at the Tl L_3-edge (12 658 eV) were performed at the LISA beamline BM 08 (d'Acapito et al. 2019) at the European Synchrotron Radiation Facility (ESRF), Grenoble, France. Measurements on alum-(K) were collected in fluorescence mode by means of a 12-elements solid state detector (high-purity germanium; Puri et al. 2019). A fixed exit sagittally focusing monochromator (d'Acapito et al. 2014) with a pair of Si (311) crystals was used; Pd coated mirrors were used for harmonics rejection ($E_{cutoff} \approx 18$ keV). A few grains of alum-(K) were powdered, mixed with cellulose, and pressed in a pellet using an amount of material such as to keep the maximum total absorption

Table 1. Chemical data for alum-(K) and voltaite from the Fornovolasco mining complex

	Alum-(K)[a]	Voltaite Dark (n = 15)			Voltaite Bright (n = 5)		
Oxide	wt%	wt%	range	e.s.d.	wt%	range	e.s.d.
SO_3	33.27	46.35	45.03–46.84	0.48	45.98	45.30–46.86	0.66
Al_2O_3	8.79	2.43	2.34–2.54	0.06	2.39	2.32–2.46	0.06
FeO_{tot}	–	22.85	22.14–23.95	0.63	23.83	23.47–24.21	0.32
Fe_2O_3	2.24	11.90			11.74		
FeO	–	12.14			13.27		
MgO	–	1.86	1.34–2.30	0.28	1.77	1.48–1.99	0.20
MnO	–	2.18	1.59–2.53	0.24	0.98	0.82–1.20	0.16
K_2O	7.13	4.36	3.19–5.23	0.44	4.62	4.27–5.12	0.31
Tl_2O	4.42	2.88	2.39–3.39	0.29	3.30	2.83–3.86	0.41
H_2O_{calc}	44.15	15.74			15.62		
Total	100.00	99.84			99.67		

Note: H_2O calculated on the basis of stoichiometry. In the chemical analyses of voltaite, the FeO and Fe_2O_3 contents were calculated in order to match the atomic ratio $(Mg + Mn + Fe^{2+})/(Al + Fe^{3+}) = 5/4$.
[a] Normalized to total = 100 wt%.

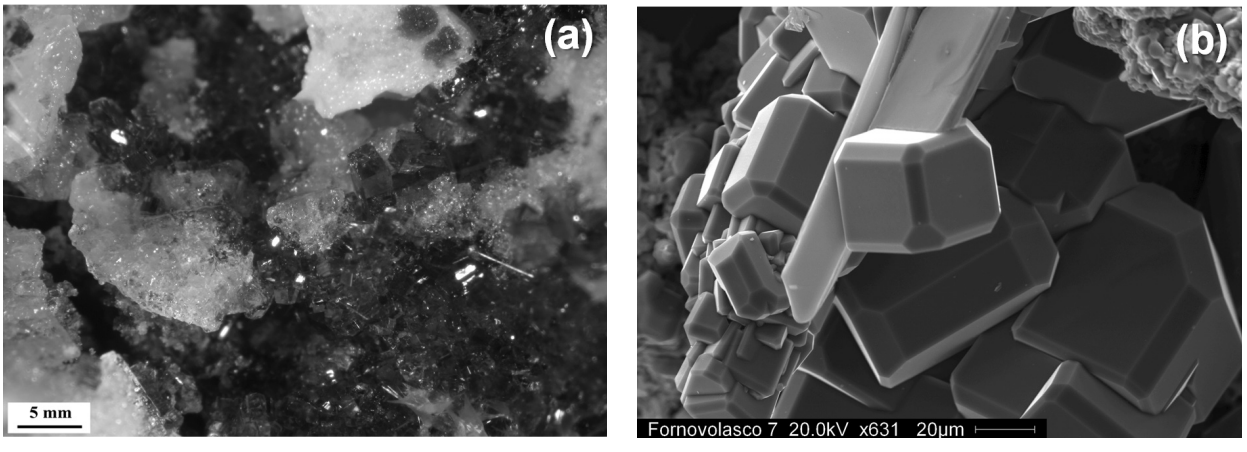

Figure 1. Tl-bearing sulfates from the Fornovolasco mining complex. (**a**) Alum-(K) as colorless crystalline masses associated with römerite, copiapite, and minor voltaite. (**b**) Voltaite, {100} individuals with minor {111} and {110} faces, associated with a tabular crystal of alunogen.

Table 2. Crystal data and summary of parameters describing data collection and refinement for alum-(K) and voltaite

	Alum-(K)	Voltaite
Crystal data		
X-ray formula	$(K_{0.879}Tl_{0.121})(Al_{0.877}Fe_{0.123})(SO_4)_2(H_2O)_{12}$	$(K_{1.872}Tl_{0.128})(Fe_{1.964}Mg_{0.036})(Fe_{2.238}Mg_{0.762})Al(SO_4)_{12}(H_2O)_{18}$
Crystal size (mm)	0.15 x 0.12 x 0.10	0.08 x 0.08 x 0.07
Cell setting, space group	$Pa\bar{3}$	$Fd\bar{3}c$
a (Å)	12.2030(2)	27.2635(18)
V (Å^3)	1817.19(9)	20265(4)
Z	4	16
Data collection and refinement		
Radiation, wavelength (Å)	Mo$K\alpha$, λ = 0.71073	Mo$K\alpha$, λ = 0.71073
Temperature (K)	293	293
Maximum observed 2θ (°)	54.95	54.93
Measured reflections	10598	19025
Unique reflections	705	976
Reflections F_o>4σ(F_o)	648	817
R_{int} after absorption corr.	0.0284	0.0626
$R\sigma$	0.0110	0.0199
Range of h, k, l	$-15 \le h \le 14$ $-15 \le k \le 11$ $-15 \le l \le 15$	$-35 \le h \le 34$ $-35 \le k \le 26$ $-30 \le l \le 35$
R_1 (F_o>4 σ F_o)	0.0351	0.0434
R_1 (all data)	0.0385	0.0548
wR_2 (on F_o^2)	0.0867	0.1263
Goodness of fit	1.192	1.162
Number of l.s. parameters	61	87
Maximum and min. residual peak (e/Å^3)	0.29 [at 0.85 Å from O(4)A] −0.31 [at 0.08 Å from O(3)A]	1.26 [at 1.19 Å from Ow(6)] −0.39 [at 0.61 Å from H(53)]

(μ) around 1.5. Voltaite was measured with the new BM08 setup (d'Acapito et al. 2019), using a pair of Si (111) flat crystals and Si coated focusing mirrors ($E_{cutoff} \approx$ 16 keV); the beam size on the sample was ≈200 × 200 μm^2. Measurements were taken on a grain of voltaite in fluorescence mode using a Si photodiode detector. Pellets of Tl_2O_3 and Tl_2SO_4 were also measured as model compounds in transmission mode. A reference Se foil (K-edge = 12 657.8 eV) was also measured at the same time to accurately calibrate the energy. The software ATHENA (Ravel and Newville 2005) was used to average multiple spectra. Standard procedures (Lee et al. 1981) were followed to extract the structural extended X-ray absorption fine structure (EXAFS) signal [$k\cdot\chi(k)$]: pre-edge background removal, spline modeling of bare atomic background, edge step normalization using a far above the edge region, and energy calibration. Model atomic clusters centered on the absorber atom were obtained by ATOMS (Ravel 2001) using the crystallographic structure reported in this paper for alum-(K) and voltaite; theoretical amplitude and phase functions were generated using the FEFF8 code (Ankudinov et al. 1998). EXAFS spectra were fitted through the ARTEMIS software (Ravel and Newville 2005) in the Fourier transform (FT) space.

Intensity data of alum-(K) and voltaite were collected using a Bruker Smart Breeze single-crystal diffractometer operating at 50 kV and 30 mA and equipped with an air-cooled CCD detector. Graphite-monochromatized Mo$K\alpha$ radiation was used. The detector-to-crystal working distance was set to 50 mm. Intensity data were integrated and corrected for Lorentz, polarization, background effects, and absorption using the package of software APEX 2 (Bruker AXS Inc. 2004). The crystal structures of both minerals were refined using SHELXL-2018 (Sheldrick 2015), starting from the atomic coordinates given by Ballirano (2015) and by Mereiter (1972) for alum-(K) and voltaite, respectively. Taking into account the results of chemical analyses (see below), the following neutral scattering curves, taken from the International Tables for Crystallography (Wilson 1992), were used: for alum-(K), K vs. Tl at the K site, Al vs. Fe at the Al site, S at the S site, and H at the H sites; for voltaite, K vs. Tl at the K site, Fe vs. Mg at the M(1) and M(2) sites, Al at the Al site, and H at the H sites, respectively. Fully ionized scattering curves were used for O atoms at the O sites in both crystal structure refinements. In the structural refinement of both minerals, a soft restraint on the O–H distance was applied [0.95(2) Å], to avoid too short O–H distances. In voltaite, the H atoms belonging to the disordered H_2O groups were not located. After several cycles of anisotropic refinement (with the exception of H atoms, which were refined isotropically), the crystal structure refinements of alum-(K) and voltaite converged to R_1 = 0.0351 [for 648 unique reflections with $F_o > 4\sigma(F_o)$ and 61 refined parameters] and 0.0434 [for 817 unique reflections with $F_o > 4\sigma(F_o)$ and 87 refined parameters], respectively. Details of data collections and crystal structure refinements are given in Table 2. Fractional atomic coordinates, site occupancies, and displacement parameters are reported in Table 3, whereas Table 4 shows selected bond distances for alum-(K) and voltaite. Weighted bond-valence sums (BVS, in valence unit, v.u.), calculated on the basis of the bond parameters given by Brese and O'Keeffe (1991), are given in Table 5.

Table 3. Site occupancy factors (s.o.f.), fractional atom coordinates, and isotropic (*) or equivalent isotropic displacement parameters (in Å^2) for alum-(K) and voltaite

Site	Wyckoff position	s.o.f.	x/a	y/b	z/c	$U_{eq/iso}$
Alum-(K)						
K	4*b*	$K_{0.879(2)}Tl_{0.121(2)}$	½	½	½	0.0526(4)
Al	4*a*	$Al_{0.877(8)}Fe_{0.123(8)}$	0	0	0	0.0178(4)
S	8*c*	$S_{1.00}$	0.30852(4)	0.30852(4)	0.30852(4)	0.0225(3)
Ow(1)	24*d*	$O_{1.00}$	0.15320(12)	0.01817(13)	−0.01744(13)	0.0256(4)
Ow(2)	24*d*	$O_{1.00}$	0.04621(16)	0.13636(15)	0.30100(15)	0.0374(5)
O(3)	8*c*	$O_{0.770(3)}$	0.2403(2)	0.2403(2)	0.2403(2)	0.0658(15)
O(3)A	8*c*	$O_{0.230(3)}$	0.3761(7)	0.3761(7)	0.3761(7)	0.0658(15)
O(4)	24*d*	$O_{0.770(3)}$	0.2652(2)	0.4209(2)	0.3115(2)	0.0461(8)
O(4)A	24*d*	$O_{0.230(3)}$	0.2873(8)	0.2041(7)	0.3646(8)	0.0461(8)
H(11)	24*d*	$H_{1.00}$	0.205(2)	0.028(3)	0.041(2)	0.066(11)*
H(12)	24*d*	$H_{1.00}$	0.187(2)	0.044(3)	−0.083(2)	0.068(11)*
H(21)	24*d*	$H_{1.00}$	−0.002(3)	0.195(2)	0.291(3)	0.069(11)*
H(22)	24*d*	$H_{1.00}$	0.115(2)	0.168(4)	0.300(4)	0.100(16)*
Voltaite						
K	32*b*	$K_{0.936(3)}Tl_{0.064(3)}$	¼	¼	¼	0.0358(9)
M(1)	32*c*	$Fe_{0.982(14)}Mg_{0.018(14)}$	0	0	0	0.0152(5)
M(2)	96*g*	$Fe_{0.746(10)}Mg_{0.254(10)}$	¼	0.10274(3)	−0.10274(3)	0.0170(4)
Al	16*a*	$Al_{1.00}$	⅛	⅛	⅛	0.0129(9)
S	192*h*	$S_{1.00}$	0.23742(4)	0.27552(4)	0.11854(4)	0.0148(3)
O(1)	192*h*	$O_{1.00}$	0.24984(13)	0.24646(13)	0.07377(12)	0.0230(7)
O(2)	192*h*	$O_{1.00}$	0.22466(15)	0.32600(13)	0.10409(14)	0.0298(9)
O(3)	192*h*	$O_{1.00}$	0.19484(15)	0.25393(15)	0.14332(16)	0.0391(10)
O(4)	192*h*	$O_{1.00}$	0.28004(14)	0.27514(15)	0.15208(13)	0.0303(9)
Ow(5)	192*h*	$O_{1.00}$	0.18263(11)	0.41982(12)	0.12142(11)	0.0163(7)
Ow(6)	192*h*	$O_{0.25}$	0.0896(5)	0.1464(6)	0.0703(5)	0.030(2)
Ow(7)	192*h*	$O_{0.25}$	0.0692(5)	0.0889(6)	0.1041(5)	0.030(2)
H(52)	192*h*	$H_{1.00}$	0.172(6)	0.424(3)	0.1530(14)	0.08(2)*
H(53)	192*h*	$H_{1.00}$	0.167(3)	0.433(3)	0.094(2)	0.08(2)*

Note: U_{eq} is defined as one third of the trace of the orthogonalized U^{ij} tensor.

Table 4. Selected bond distances (in Å) for alum-(K) and voltaite

Alum-(K)			
K–O(3)A (×2)	2.618(16)	S–O(3)A	1.429(16)
K–Ow(2) (×6)	2.9974(19)	S–O(3)	1.442(5)
		S–O(4)A (×3)	1.469(8)
Al–Ow(1) (×6)	1.8946(14)	S–O(4) (×3)	1.470(2)
Voltaite			
K–O(4) (×6)	2.875(4)	Al–Ow(6)(×6)	1.868(14)
K–O(3) (×6)	3.276(5)	Al–Ow(7) (×6)	1.900(13)
M(1)–O1 (×6)	2.014(3)		
		S–O(3)	1.466(4)
M(2)–Ow/5) (×2)	2.003(3)	S–O(2)	1.473(4)
M(2)–O(2) (×2)	2.062(4)	S–O(4)	1.479(4)
M(2)–O(4) (×2)	2.101(4)	S–O(1)	1.494(4)

Results and discussion

Alum-(K): crystal structure, sulfate disorder, and thallium speciation

Alum-(K), $KAl(SO_4)_2\cdot 12H_2O$, belongs to the alum group, a series of cubic minerals and synthetic compounds characterized by the general formula $X^+Y^{3+}(T^{6+}O_4)_2\cdot 12H_2O$, where X = Na, K, Rb, Cs, Tl, NH_4, NH_3CH_3, NH_3OH, etc.; Y = Al, Cr, Fe, Ga, In, Ru, etc.; and T = S or Se (e.g., Nyburg et al. 2000; Ballirano 2015). In addition to alum-(K), other natural members of the alum group are alum-(Na) (X = Na, Y = Al), lanmuchangite (X = Tl, Y

TABLE 5a. Weighted bond valences for alum-(K) and voltaite, in valence units (v.u.)

	Alum-(K)						
Site	Ow(1)	Ow(2)	O(3)	O(3)A	O(4)	O(4)A	Σcations
K		$^{6x\rightarrow}$0.09		0.06			0.60
Al	$^{6x\rightarrow}$0.54						3.24
S			1.26	0.39	$^{3x\rightarrow}$1.17	$^{3x\rightarrow}$0.35	6.21
Σanions	0.54	0.09	1.64[a]	1.75[a]	1.52[a]	1.52[a]	
H-bonds	–0.27	+0.27	+0.19	–	+0.28	+0.17	
	–0.28[b], –0.17[c]	–0.17[d]	+0.19		+0.20	+0.16	
		–0.19[e]	+0.19			+0.10	
$\Sigma anions_{corr}$	–0.01[b], 0.10[c]	0.00	2.21[a]	1.75[a]	2.00[a]	1.95[a]	

[a] Assuming the full occupancy of the corresponding O site.
[b] O(4) acceptor
[c] O(4)A acceptor
[d] Weighted between O(3) (0.19, s.o.f. 0.77) and O(4)A (0.11, s.o.f. 0.23).
[e] Weighted between O(4) (0.20, s.o.f. 0.77) and O(4)A (0.16, s.o.f. 0.23).

TABLE 5b. Weighted bond valences for alum-(K) and voltaite, in valence units (v.u.)

	Voltaite						
Site	O(1)	O(2)	O(3)	O(4)	Ow(5)	Ow(6)/ Ow(7)	Σcations
K			$^{6x\rightarrow}$0.04	$^{6x\rightarrow}$0.13			1.02
M(1)	$^{6x\rightarrow}$0.50						3.00
M(2)		$^{2x\rightarrow}$0.41		$^{2x\rightarrow}$0.37	$^{2x\rightarrow}$0.48		2.52
Al						$^{3x\rightarrow}$0.56	3.21
						$^{3x\rightarrow}$0.51	
S	1.42	1.50	1.53	1.48			5.93
Σanions	1.92	1.91	1.57	1.98	0.48	0.56	
						0.51	
H-bonds	–	+0.13	+0.14	–	–0.13	–	–
			+0.40/+0.30/ +0.20/+0.18[a]	–0.14			
$\Sigma anions_{corr}$	1.92	2.04	2.11/2.01/ 1.91/1.89	1.98	0.21	–0.14/+0.13	

[a] Values calculated assuming the full occupancy at Ow(6) and Ow(7).

= Al), tschermigite (X = NH_4, Y = Al), and probably lonecreekite (X = NH_4, Y = Fe). The crystal structure of alum-(K) was first solved by Cork (1927) and later reinvestigated by Beevers and Lipson (1934). In agreement with Lipson (1935), alums are divided into three types, i.e., α-, β-, and γ-type, depending on the orientation of the SO_4 group. This polymorphism seems to be related to the occurrence of monovalent cations with medium (α), small (β), and large (γ) ionic radii. Larson and Cromer (1967) refined the crystal structure of synthetic α-alums (X = K, Rb, and NH_4) and pointed out the occurrence of SO_4 disorder.

The chemical formula of the studied sample of alum-(K), on the basis of 8 O atoms per formula unit (apfu) and assuming the occurrence of 12 H_2O groups, is $(K_{0.74}Tl_{0.10})_{\Sigma 0.84}(Al_{0.84}Fe_{0.14})_{\Sigma 0.98}S_{2.03}O_8 \cdot 12H_2O$. The significant deficit of (K+Tl) can be partly related to the low quality of chemical analysis and K migration under the electron beam (e.g., Craw 1981; van der Pluijm et al. 1988), but it could also mask the presence of an undetected light constituent, such as NH_4. This Tl-bearing sample has a unit-cell parameter (~12.20 Å) intermediate between those of pure synthetic $KAl(SO_4)_2 \cdot 12H_2O$ (hereafter KAl-alum), 12.1640(5) Å, and pure synthetic $TlAl(SO_4)_2 \cdot 12H_2O$ (hereafter TlAl-alum), 12.2305(5) Å. It is worth noting that, if one assumes a linear increase of the unit-cell parameter from KAl-alum to TlAl-alum, the measured *a* value should correspond to ca. 0.40 Tl apfu, neglecting minor Fe^{3+}-to-Al^{3+} substitution. Chemical data, as well as crystal structure refinement (see below), do not support such a high Tl content, and it is likely that the substitution of Al^{3+} by Fe^{3+} could contribute to the increase of the unit-cell parameter. However, another component, characterized by a large ionic radius and low *Z* number, should be likely present. As discussed below, this additional component is represented by $(NH_4)^+$, whose ionic radius is similar to that of Tl^+ (compare isotypic compounds TlCl and NH_4Cl, Roberts et al. 2006). Therefore, the increase in the unit-cell parameter is not only related to the $K^+ \rightarrow Tl^+$ substitution, but also to the replacement of K^+ by NH_4^+ and Al^{3+} by Fe^{3+}.

The crystal structure of the studied sample agrees with previous determinations (e.g., Ballirano 2015): alum-(K) is formed by isolated $Al(H_2O)_6$ octahedra, $K(H_2O)_6$ polyhedra, and SO_4 groups (Fig. 2). Hydrogen bonds play an important role in stabilizing the crystal structure.

Two SO_4 configurations have been observed, in agreement with previous studies. However, whereas the *k* disorder parameter [i.e., the site occupancy factor of O(3) and O(4) sites] is ~0.7 in KAl-alum, a higher value, close to ~0.8, occurs in Tl-bearing alum-(K). This is in keeping with the larger ionic radius of Tl^+ (as well as NH_4^+) with respect to K^+ (1.50 vs. 1.38 Å in sixfold coordination for Tl^+ and K^+, respectively, according to Shannon 1976). Indeed, the larger the ionic radius of the M^+ cation, the higher the *k* value, e.g., 0.697 and 0.843 in KAl and TlAl synthetic alums (Nyburg et al. 2000). The most probable SO_4 configuration (77%) has average bond distance 1.463 Å, with distances ranging from 1.442(5) to 1.470(2) Å; the less probable configuration (23%) has a shorter average bond distance, i.e., 1.459 Å, with distances in the range 1.429(16)–1.469(8) Å. These values can be compared with the results of Nyburg et al. (2000) and Ballirano (2015), i.e., 1.468 and 1.466 Å for the more frequent configuration, and 1.450 Å for the less frequent one. Moreover, these values can be compared with the grand <S–O> distance of 1.473 Å reported by Hawthorne et al. (2000). The shortening of S–O distances in alum-(K) has been attributed to libration effects (Nyburg et al. 2000). The corresponding weighted bond-valence sum is 6.21 valence unit (v.u.); actually, it is 6.19 and 6.25 v.u. for the more and less frequent configurations, respectively. The occurrence of two distinct configurations of SO_4 group results in the appearance, in the Raman spectrum of alum-(K) (Fig. 3a), of two close bands having different intensities; such a difference is directly related to differences in the site occupancy at the O(3)/O(3)A and O(4)/O(4)A sites. The integrated intensity ratio between the two bands related to the ν_1 stretching mode of SO_4 groups (Fig. 3a) is 75/25, very close to the 77/23 ratio obtained through single-crystal structure refinement. The Raman spectrum of alum-(K) shows other spectral features related to vibrational modes of SO_4 groups (Fig. 3a), in agreement with Frost and Kloprogge (2001).

The Al–O bond distance, 1.8946(14) Å, is larger than those observed by Nyburg et al. (2000) and Ballirano (2015), i.e., 1.875(1) and 1.868(2) Å. This is likely the result of the replacement of Al^{3+} by Fe^{3+}, giving the site occupancy $(Al_{0.88}Fe_{0.12})$, in good agreement with chemical data. The occurrence of Fe^{3+} in alum-(K) suggests the possible existence of the end-member composition $KFe^{3+}(SO_4)_2 \cdot 12H_2O$, the K-analog of lonecreekite (Martini 1983). On the basis of these s.o.f., the calculated BVS is 3.24 v.u.

The K site hosts K^+, partially replaced by Tl^+ and $(NH_4)^+$; the refined site occupancy is $(K_{0.88}Tl_{0.12})$. The occurrence of NH_4 is confirmed by FTIR spectroscopy showing a band occurring at

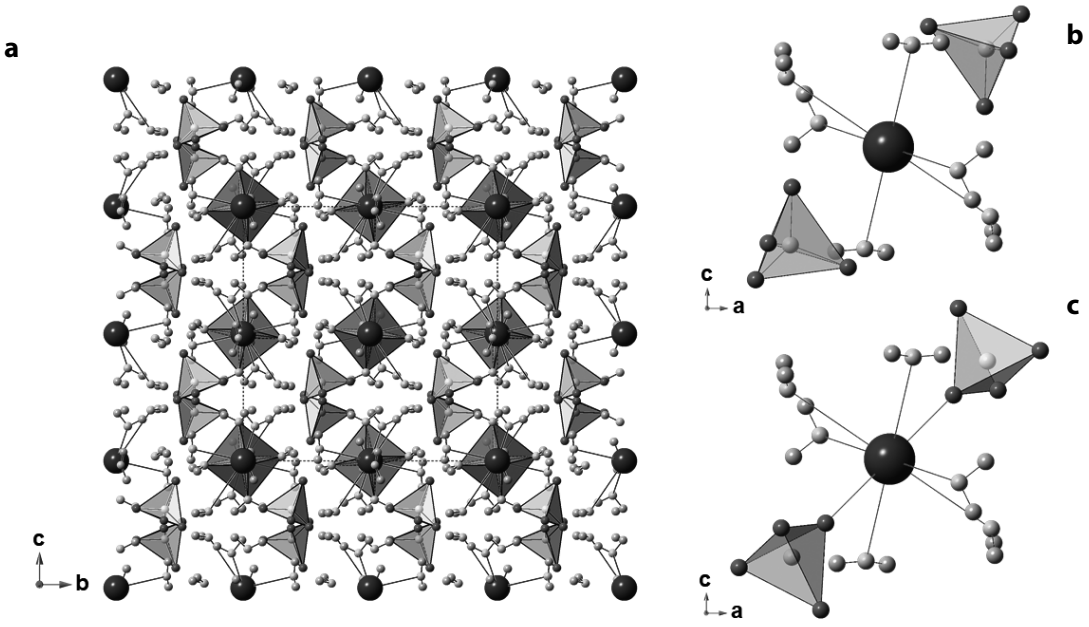

Figure 2. Crystal structure of alum-(K), as seen down **a**, and the two different SO_4 configurations, not bonded (**b**) and bonded to K^+ (**c**). Dark gray and gray polyhedra represent Al and S sites, respectively. Dark gray, gray, and light gray small circles represent O, H, and Ow sites, respectively, whereas the K site is shown as large dark gray circles.

1443 cm^{-1} (Fig. 3b), in agreement with the value reported in tschermigite (e.g., Zhitova et al. 2019). These monovalent cations are coordinated by six H_2O groups in an almost flat "crown" coordination, with bond distance of 2.9974(19) Å. This distance is longer than that observed in KAl-alum by Nyburg et al. (2000) and Ballirano (2015), i.e., 2.954(1) and 2.947(2) Å, respectively, as a result of the replacement of K^+ by the larger Tl^+ and NH_4^+. Two additional bond distances are associated with the occurrence of the less frequent SO_4 configuration, i.e., 2.618(16) Å, to be compared with the value reported by Nyburg et al. (2000) and Ballirano (2015), i.e., 2.636(5) and 2.6348(18) Å. Larson and Cromer (1967) suggested that the K site may be split into two sub-positions, to avoid the K–O(3)A bonds. However, as pointed out by Ballirano (2015), this model would result in a too low BVS [0.66 v.u. according to Ballirano 2015; 0.58 v.u. in the present refinement of Tl-bearing alum-(K)]. Consequently, this author proposed that a sevenfold coordination or, alternatively, an eightfold coordination, may occur, giving BVS of 0.91 and 1.16 v.u., respectively (0.86 and 1.14 v.u. in the present refinement). Following Ballirano (2015), a sevenfold coordination seems more likely, providing an overall charge neutrality to the crystal structure. In each unit cell there are four K^+ cations and eight SO_4 groups; consequently, to achieve a sevenfold coordination for all K^+ ions, a k value of 0.5 would be necessary. In Tl-bearing alum-(K) the k disorder parameter of 0.77 corresponds to 1.84 SO_4 groups available for bonding to K^+ through O(3)A, i.e., 46% and

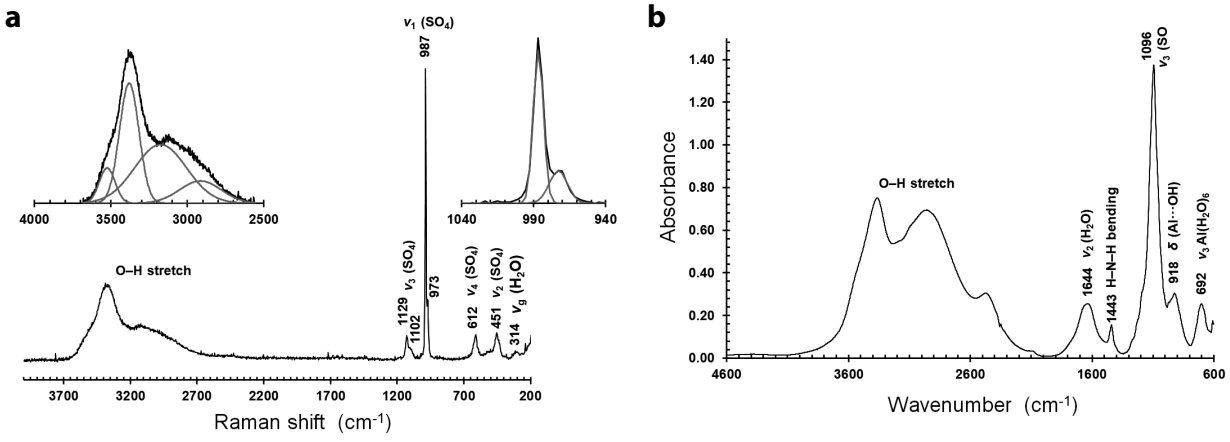

Figure 3. Micro-Raman (**a**) and FTIR (**b**) spectra of alum-(K) and band interpretation. The deconvolution of the O–H stretching region and the ν_1 (SO_4) modes in the Raman spectrum are shown on upper left and right in **a**, respectively.

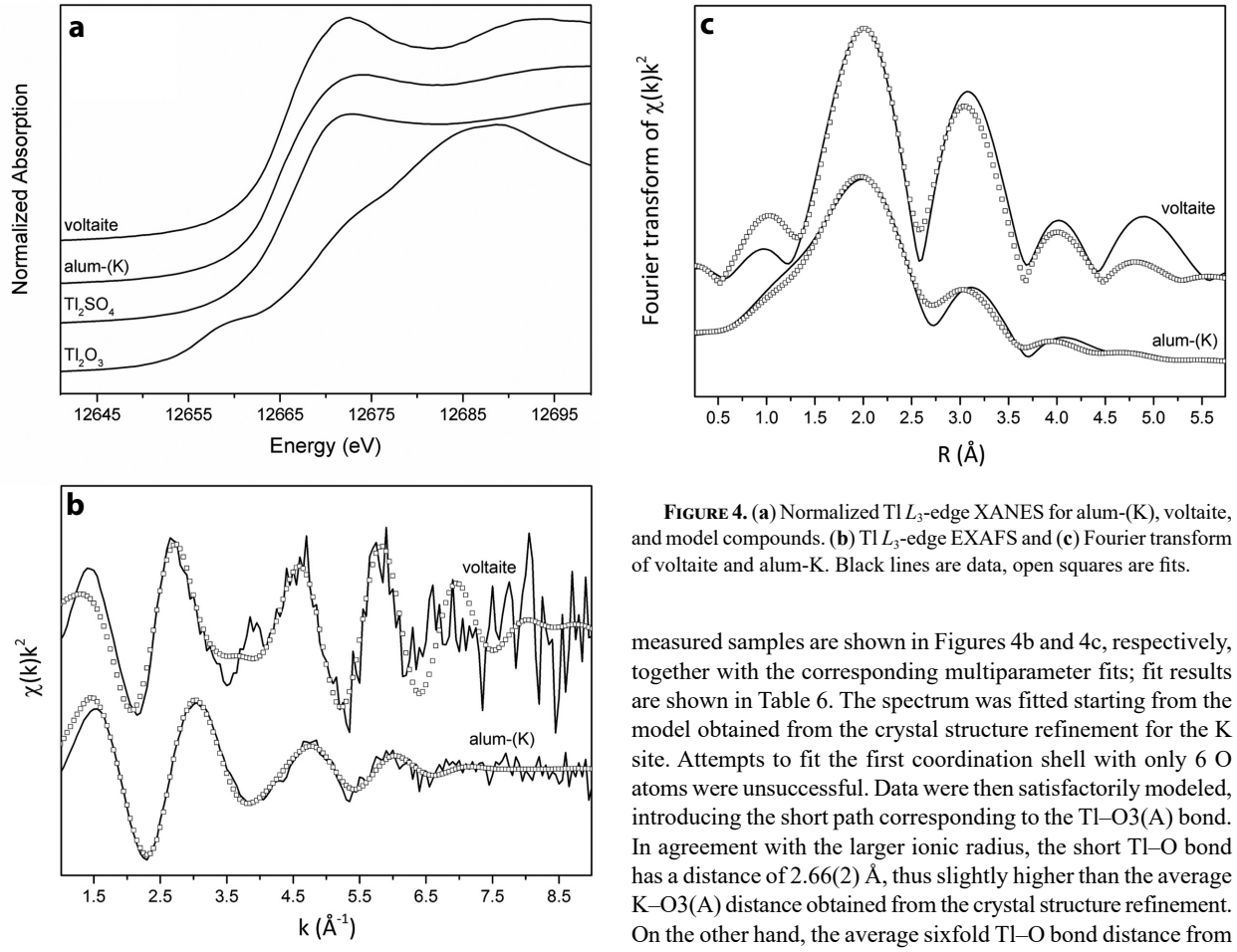

Figure 4. (**a**) Normalized Tl L_3-edge XANES for alum-(K), voltaite, and model compounds. (**b**) Tl L_3-edge EXAFS and (**c**) Fourier transform of voltaite and alum-K. Black lines are data, open squares are fits.

54% of sevenfold and sixfold coordinated K sites, respectively. The "average" K site would have a BVS of 0.71 v.u., a value still relatively low that confirms the occurrence of another large cation, i.e., NH_4^+. Unfortunately, the quality of chemical data and the small amount of available material did not allow to quantify the NH_4 content. Some hints can be obtained from the crystal structure refinement. The refined site scattering at the K site is 26.4 electrons per formula unit (epfu). Chemical data indicate the occurrence of a deficit of cations at the K site and spectroscopic data confirm the occurrence of $(NH_4)^+$. Assuming that the difference from the full occupancy is represented by $(NH_4)^+$ ions, the site population $[K_{0.74}(NH_4)^+_{0.16}Tl_{0.10}]$ can be proposed, corresponding to a site scattering of 23.3 epfu. Finally, the K site shows a relatively large anisotropic displacement ellipsoid, with the longest axis in the direction of O(3)A. Consequently, a slight shift toward O(3)A may occur, increasing its BVS.

To study the local environment of thallium within the crystal structure of alum-(K), XAS studies were performed at the Tl L_3 edge on the "LISA" CRG beamline at ESRF (d'Acapito et al. 2019). The XANES spectrum of alum-(K) is shown in Figure 4a, together with the spectra of reference compounds. The position and shape of the main absorption edge confirm that Tl occurs as Tl^+, with the XANES region fairly resembling that of Tl_2SO_4. Thallium L_3-edge EXAFS and Fourier transform of measured samples are shown in Figures 4b and 4c, respectively, together with the corresponding multiparameter fits; fit results are shown in Table 6. The spectrum was fitted starting from the model obtained from the crystal structure refinement for the K site. Attempts to fit the first coordination shell with only 6 O atoms were unsuccessful. Data were then satisfactorily modeled, introducing the short path corresponding to the Tl–O3(A) bond. In agreement with the larger ionic radius, the short Tl–O bond has a distance of 2.66(2) Å, thus slightly higher than the average K–O3(A) distance obtained from the crystal structure refinement. On the other hand, the average sixfold Tl–O bond distance from EXAFS results is significantly shorter than that observed in the structural refinement [2.84(2) vs. 2.997(2) Å], thus extremely close to the ideal value of 2.835 Å that would lead to a BVS of 1 v.u. for Tl in sixfold coordination. This discrepancy may be related to a locally higher value of the *k* disorder parameter around Tl atoms. The multiparameter fit results highlight in any case that the contribution of the Tl–O3(A) bond is not negligible; the weak EXAFS signal, however, prevents us from obtaining an estimation of the probability for the short Tl–O3(A) path to occur. The second peak in the Fourier transform corresponds to a further Tl–O shell at 3.82(2) Å that can be interpreted as an interaction with the O(4) atoms of the SO_4 group in the more likely α orientation.

The BVS at O sites confirm the occurrence of H_2O groups at Ow(1) and Ow(2), and O^{2-} anions at O(3)/O(3)A and O(4)/O(4)A.

Table 6. EXAFS multiparameter fit details for alum-(K) and voltaite, Tl L_3-edge

	S_0^2	ΔE_0 (eV)	Path	N	R (Å)	σ^2 (Å^2)	*k* range (Å^{-1})	R-factor
Alum-(K)	1.1(2)	−7(1)	Tl-O	2	2.66(2)	0.034(5)	2.0–6.3	0.015
			Tl-O	6	2.84(2)	//	//	
			Tl-O	6	3.79(3)	//	//	
Voltaite	0.8(3)	3(1)	Tl-O	6	2.89(2)	0.016(6)	2.0–6.1	0.039
			Tl-S	6	3.61(3)	0.018(5)	//	

Notes: S_0^2 = amplitude reduction factor, DE_0 = shift of the energy origin, R = path length, N = path degeneracy, σ^2 = Debye-Waller factor. Errors, as calculated by ARTEMIS, are indicated in parentheses. *R*-factor is defined as $R = \Sigma(|\text{data} - \text{fit}|^2)/\Sigma(|\text{data}|^2)$.

Table 7. Bond lengths (Å), angles (°), and bond strengths (v.u.) for H-bonds in alum-(K) and voltaite

Donor (*D*)	*D*–H	Acceptor (*A*)	H···*A*	*D*–H···*A* angle	*D*···*A*	Bond strength[a]
Alum-(K)						
Ow(1)–H(11)	0.963(19)	Ow(2)	1.663(19)	176(4)	2.625(2)	0.27
Ow(1)–H(12)	0.950(18)	O(4)	1.663(10)	170(3)	2.604(3)	0.28
Ow(1)–H(12)	0.950(18)	O(4)A	1.95(2)	157(3)	2.848(10)	0.17
Ow(2)–H(21)	0.929(19)	O(4)	1.84(2)	165(4)	2.749(3)	0.20
Ow(2)–H(21)	0.929(19)	O(4)A	1.99(2)	161(3)	2.882(8)	0.16
Ow(2)–H(22)	0.92(2)	O(3)	1.91(3)	158(4)	2.787(3)	0.19
Ow(2)–H(22)	0.92(2)	O(4)A	2.29(3)	155(4)	3.153(11)	0.11
Voltaite						
Ow(5)–H(52)	0.92(2)	O(2)	2.07(2)	173(15)	2.990(5)	0.13
Ow(5)–H(53)	0.92(2)	O(3)	2.13(5)	148(7)	2.955(5)	0.14

[a] Calculated according to Ferraris and Ivaldi (1988).

The latter are acceptors of H-bonds from Ow(1) and Ow(2), the only exception being represented by O(3)A, which is not involved in any H-bond. Table 7 gives the geometrical features of H-bonds in the studied sample, agreeing with previous determinations (e.g., Nyburg et al. 2000). Micro-Raman spectrum of Tl-bearing alum-(K) (Fig. 3) shows a broadband in the O–H stretching region. Its deconvolution reveals the occurrence of at least four main bands, at 2916, 3176, 3381, and 3526 cm^{-1}. Using the relation proposed by Libowitzky (1999) between O–H stretching frequencies and O···O distances, the following distances can be calculated (in Å): 2.63, 2.70, 2.79, and 2.94, to be compared with the values given in Table 7. Since all H_2O groups are bonded to K or to Al, the chemical formula of alum-(K) should be correctly written as $KAl(SO_4)_2(H_2O)_{12}$.

Voltaite: crystal-chemistry and thallium speciation

Voltaite, $K_2Fe^{2+}_5Fe^{3+}_3Al(SO_4)_{12}\cdot 18H_2O$, is a member of the voltaite group, formed by cubic ($Fd\bar{3}c$) and tetragonal ($I4_1/acd$) species having general formula $X_2Y^{2+}_5Z^{3+}_3Al(TO_4)_{12}\cdot 18H_2O$, where $X = K^+$, $(NH_4)^+$, Tl^+, Rb^+; $Y = Fe^{2+}$, Mg^{2+}, Zn^{2+}, Mn^{2+}, Cd^{2+}, Co^{2+}; $Z = Fe^{3+}$; and $T = S^{6+}$. In some synthetic compounds, Al can be replaced by Fe^{3+}, e.g., in "K-Mg-Fe^{3+}-voltaite" described by Schwarte and Fischer (1989). In addition to voltaite, other natural members of this group are ammoniomagnesiovoltaite [$X = (NH_4)^+$, $Y = Mg^{2+}$], ammoniovoltaite [$X = (NH_4)^+$, $Y = Fe^{2+}$], magnesiovoltaite ($X = K^+$, $Y = Mg^{2+}$), and zincovoltaite ($X = K^+$, $Y = Zn^{2+}$). The group is completed by pertlikite, which shows a tetragonal superstructure owing to the ordering of divalent cations (Ertl et al. 2008). Other compositions were synthesized (e.g., Gossner and Fell 1932; Gossner and Drexler 1933; Gossner and Besslein 1934).

Backscattered electron images of voltaite from Fornovolasco revealed the occurrence of a complex chemical zoning (see Supplementary Material[1]). The chemical formulas of the darker and brighter domains, recalculated on the basis of 66 O apfu, taking into account the data given in Table 1, are $(K_{1.91}Tl_{0.28})_{\Sigma 2.19}(Fe^{2+}_{3.48}Mg_{0.95}Mn_{0.63})_{\Sigma 5.06}Fe^{3+}_{3.07}Al_{0.98}S_{11.92}O_{48}\cdot 18H_2O$ and $(K_{2.04}Tl_{0.32})_{\Sigma 2.36}(Fe^{2+}_{3.83}Mg_{0.91}Mn_{0.29})_{\Sigma 5.03}Fe^{3+}_{3.05}Al_{0.97}S_{11.92}O_{48}\cdot 18H_2O$, respectively.

The crystal structure of voltaite group minerals, first solved by Mereiter (1972), can be described as a heteropolyhedral framework with cavities hosting disordered $Al(H_2O)_6$ octahedra (Fig. 5a). Indeed, Al is coordinated by six H_2O groups belonging to two distinct H_2O-hosting sites, i.e., Ow(6) and Ow(7). Each ordered Al-centered octahedron is formed by three H_2O groups belonging to Ow(6) and three belonging to Ow(7) (Fig. 5b).

The framework is formed by pinwheels centered at the $^{M(1)}Fe^{3+}O_6$ octahedra; the oxygen atoms belonging to this octahedron are shared with six SO_4 groups. The S site has an average <S–O> distance of 1.478 Å, with a corresponding BVS of 5.93 v.u. In agreement with Majzlan et al. (2013), each *M*(1) position is a point in the structure of voltaite where three kröhnkite-like heteropolyhedral chains intersect. The *M*(1) site is mainly occupied by Fe,

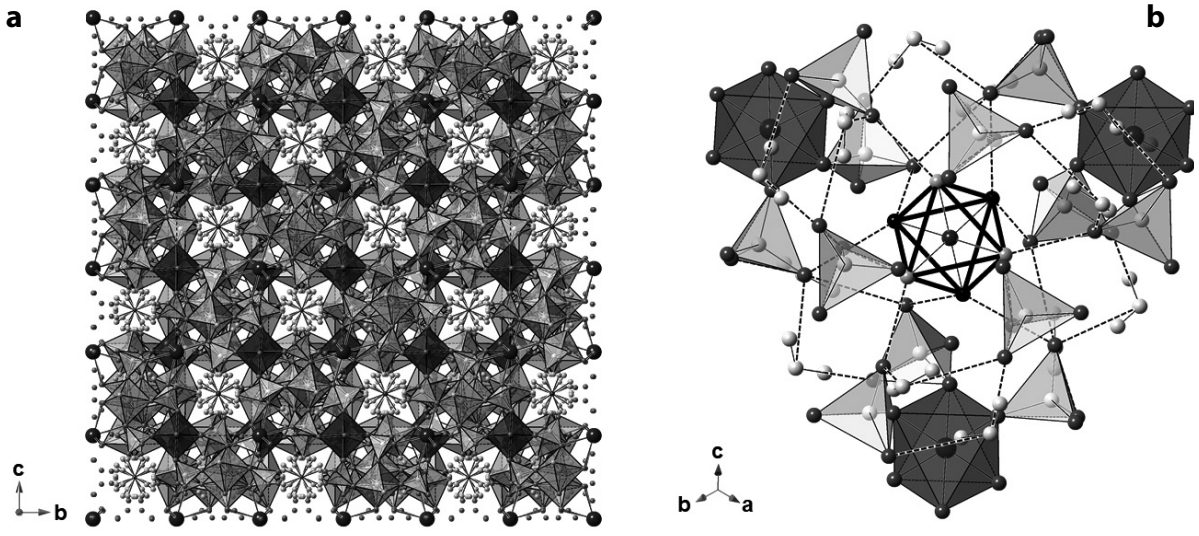

Figure 5. Crystal structure of voltaite, as seen down *a* (**a**). Polyhedra: dark gray = *M*(1) site; gray = *M*(2) site; light gray = S site. Small circles: dark gray = Al site; light gray = O atoms bonded to H atoms, forming H_2O groups; gray = O atoms. Large dark gray circles = K site. The disordered H_2O groups around Al atoms are shown. Hydrogen atoms are not shown. In **b**, an ordered Al-centered octahedron is shown down [111], along with the H-bond system. Same symbols as in **a**, with the exception of Ow(6) and Ow(7) sites, shown as gray and black circles, respectively. Dashed lines represent H-bonds.

in agreement with Majzlan et al. (2013), who reported a limited mixing between M^{2+} and M^{3+} cations in Fe^{2+}-Mg voltaites. Bond-valence sum (3.00 valence unit, v.u.) agrees with this occupancy. The slight increase in the average *M*(1)–O distance (2.014 Å), with respect to the expected value of 1.995 Å calculated using the ionic radii of $^{VI}Fe^{3+}$ and $^{II}O^{2-}$ given by Shannon (1976), assuming the full occupancy by Fe^{3+}, suggests the occurrence of Fe^{2+}. Neglecting minor Mg^{2+}, a site population $(Fe^{3+}_{0.87}Fe^{2+}_{0.13})$ can be proposed for *M*(1).

The *M*(2) site is coordinated by two H_2O groups, hosted at Ow(5), and four O^{2-} anions, and it shows an average <*M*(2)–φ> distance of 2.055 Å (where φ = O^{2-}, H_2O). In agreement with the chemical data (taking into account the inhomogeneity of the studied crystals), and considering the heterovalent substitution $^{M(1)}Fe^{3+} + {}^{M(2)}Fe^{2+} = {}^{M(1)}Fe^{2+} + {}^{M(2)}Fe^{3+}$, the idealized site population should be $(Fe^{2+}_{3.3}Fe^{3+}_{1.3}Mg_{1.0}Mn_{0.4})_{\Sigma 6}$. This site population corresponds to 141.6 electrons per formula unit (epfu), to be compared with the refined site occupancy, giving 135 epfu. This discrepancy (1.3 electron per site) is likely due to the chemical variability of the studied crystals. The bond-valence sum, 2.52 v.u., is larger than the expected value of 2.22 v.u. The Fe^{2+}/Fe^{3+} atomic ratio calculated on the basis of electron microprobe analysis agrees with the results of Mössbauer spectroscopy. The spectrum of voltaite could be accurately fitted with one Fe^{2+} and one Fe^{3+} doublet (Fig. 6). In agreement with Dyar et al. (2013), the observed doublets can be assigned to ferrous and ferric iron in octahedral coordination. The isomer shifts and the quadrupole splitting for the Fe^{2+} doublet were found at 1.31 and 1.78 mm/s, respectively. The Fe^{3+} doublet shows an isomer shift of 0.46 mm/s and a quadrupole splitting of 0.33 mm/s. These data are in accord with those reported for the synthetic sample $Fe_{40}Mg_{60}$ of voltaite by Majzlan et al. (2013) and for ammoniovoltaite (Zhitova et al. 2018). With the assumption of similar recoil-free fractions, the Mössbauer spectrum of voltaite from Fornovolasco indicates an atomic ratio Fe^{2+}/Fe_{tot} of 0.55, to be compared with 0.53 and 0.56 calculated for the darker and brighter domains observed in BSE images.

The K site has six oxygen atoms at 2.875(4) Å, and six additional very long (i.e., very weak) bonds, at 3.276(5) Å. These values can be compared with those of synthetic $K_2Fe^{2+}_5Fe^{3+}_3Al(SO_4)_{12}\cdot 18H_2O$, i.e., 2.886 and 3.293 Å, respectively. The refined site scattering agrees with chemical data, confirming a minor replacement of K by Tl. The crystal structure refinement points to a Tl/(Tl+K) atomic ratio of 0.06, to be compared with 0.13–0.14 observed through electron microprobe analyses. Actually, the occurrence of minor NH_4^+ also replacing K^+ could explain the lower observed site scattering at the K site with respect to that calculated on the basis of electron microprobe data. The occurrence of Tl in voltaite was also confirmed through XAS. As in alum-(K), the position and shape of the main absorption edge confirm that Tl is present as Tl^+. Quantitative EXAFS analysis (Table 6) shows that the local structure around Tl is in substantial agreement with the results of the single-crystal X-ray diffraction refinement, with Tl bonding ~6 O atoms at ~2.9 Å. The second shell is represented by six S atoms at ~3.6 Å. No hints of the longer Tl–O interaction at ~3.3 Å can be inferred from EXAFS data. The moderate misfit between data and fit in voltaite may be ascribed to the high degree of disorder of the structure; EXAFS provides an average information and it is, therefore, difficult to model disordered structures such as that of voltaite, especially with respect to coordination shells higher than the first.

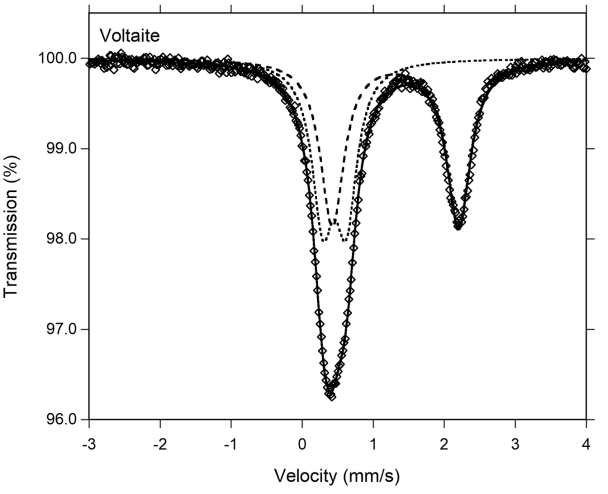

Figure 6. Mössbauer spectrum of voltaite obtained at room-temperature. Fitted absorption doublets assigned to Fe^{2+} and Fe^{3+} are indicated by dashed and dotted lines, respectively. Diamonds denote measured spectrum and black curve represents summed fitted doublets.

Thallium-rich or thallium-bearing members of the voltaite group are mainly known as synthetic products, e.g., "Tl-Fe voltaite", "Tl-Mg voltaite", and "Tl-Cd voltaite" obtained by Gossner and Fell (1932). Manilici et al. (1965) and later Götz et al. (1968) described a hydrated potassium thallium sulfate, with Tl supposed as Tl^{3+}, and named it "monsmedite". This mineral had morphology, optical properties, as well as the X-ray powder diffraction pattern very similar to those shown by voltaite group minerals. Indeed, a reexamination of this mineral by Zemann (1993), Johan et al. (2009), and Kovács-Pálffy et al. (2011) proved that "monsmedite" is voltaite with up to ~7.5 wt% Tl_2O. Its unit-cell parameter, a = 27.2587 Å (Kovács-Pálffy et al. 2011), is larger than that of synthetic $K_2Fe^{2+}_5Fe^{3+}_3Al(SO_4)_{12}\cdot 18H_2O$ (a = 27.234 Å, Mereiter 1972) and can be compared with that observed for Tl-bearing voltaite studied in this work, i.e., a = 27.2635(18) Å.

In addition, Kovács-Pálffy et al. (2011) discussed the chemical zoning of Tl-bearing voltaite, showing an increase in the Tl content from the core to the rim of the studied crystal. X-ray maps collected on the specimen from Fornovolasco showed a similar zoning (see Supplementary Material[1]). Such a chemical zoning is likely related to the relatively large estimated standard deviation (e.s.d.) of unit-cell parameter; as pointed out by Majzlan et al. (2013), the e.s.d. on the lattice parameters of voltaite are always one or two orders of magnitude higher than those of associated minerals, despite the euhedrality of voltaite (Fig. 1). X-ray maps show that both K and Tl increase from the core to the rim of the studied crystals, whereas the only detected element enriched in the core seems to be represented by Mn. Actually, the sum (K + Tl) is overestimated in electron microprobe analyses (sum of 2.19 and 2.36 apfu); such an excess was found also in several analyses reported by Majzlan et al. (2013) (up to 2.56 K per formula unit, with an average, among the studied samples of 2.17 K apfu). It seems likely that the depletion of K and Tl in the core of the studied crystals may be related to the occurrence of NH_4^+. Nitrogen was indeed detected in electron microprobe

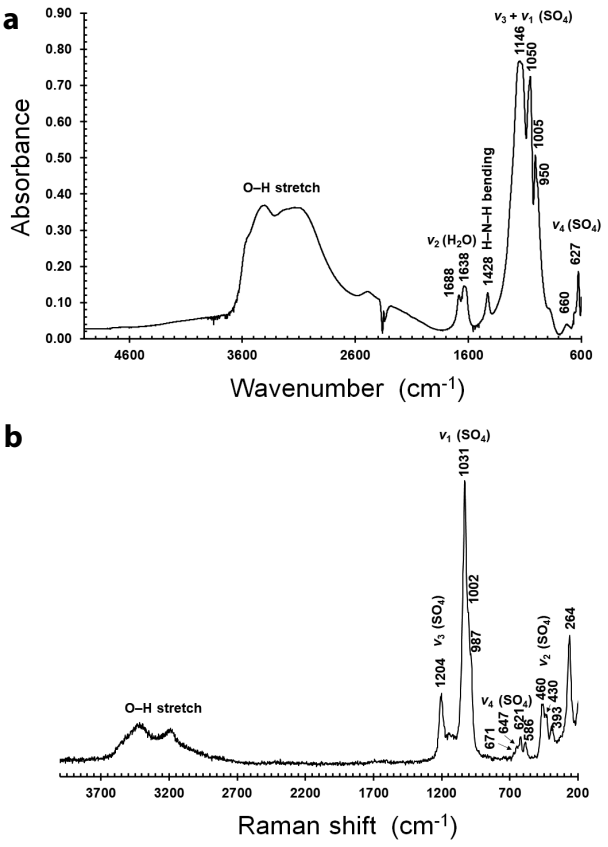

Figure 7. (**a**) FTIR and (**b**) Raman spectra of voltaite and band interpretation.

analysis but not quantified, and the characteristic band at 1428 cm^{-1} was observed in the FTIR spectrum of Tl-bearing voltaite (Fig. 7a). Majzlan et al. (2013) discussed the infrared spectra of selected samples of synthetic voltaites. Only NH_4-bearing samples show a band at 1431 cm^{-1}, related to the ν_3 mode of the NH_4 group. Similarly, Szakáll et al. (2012) and Zhitova et al. (2019) reported such a band in the FTIR spectra of ammoniomagnesiovoltaite (1431 cm^{-1}) and ammoniovoltaite (1433 cm^{-1}), respectively. Moreover, Košek et al. (2019) reported a band at 1428 cm^{-1} in the Raman spectrum of voltaite from the Anna I dump, Aldsdorf (Germany). Figure 7b shows the Raman spectrum of voltaite from Fornovolasco. No band at such a position can be observed. This is not surprising; for instance, in the Raman spectra of the NH_4-sulfates carlsonite and huizingite-(Al), the occurrence of NH_4 groups was not detected in the latter and only a very weak and broad band was observed in the former. On the contrary, FTIR clearly showed the presence of this constituent (Kampf et al. 2016).

As in previous refinements, only the H atoms bonded to Ow(5) have been located. Ow(5) is donor in two H-bonds with O(2) and O(3) (Table 6), both belonging to an (SO_4) group. In addition, every O atom hosted at O(3) is acceptor of H-bond from Ow(6) or Ow(7). Ow(6) is donor of H-bonds to two distinct oxygen atoms hosted at two symmetry-related O(3) sites, with Ow(6)···O(3) distances of 2.47 and 2.58 Å, respectively. An O···O distance of 2.47 Å is very short, being shorter than the shortest distances reported by Ferraris and Franchini-Angela (1972). However, similar distances have been reported in previous refinements of the crystal structure of voltaite group minerals (e.g., Mereiter 1972; Ertl et al. 2008), as well as in other phases, e.g., in libethenite and zincolibethenite, in which H-bonds characterized by O···O distances of 2.48 and 2.47 Å were reported, respectively (Cordsen 1978; Williams et al. 2006). Similarly, Ow(7) is donor of H-bonds to two oxygen atoms hosted at O(3), with O···O distances of 2.77 and 2.82 Å. Consequently, owing to the positional disorder affecting the Al-centered octahedra, O(3) can be involved in different H-bond configurations. It is worth noting that O(3) is acceptor of only one H-bond from Ow(6) or Ow(7); taking into account also the H-bond accepted from Ow(5), the BVS at O(3) ranges between 1.89 and 2.11 v.u. The oxygen atoms at Ow(6) and Ow(7), being donor of H-bonds, have a corrected BVS of –0.14 and +0.13 v.u., respectively.

The FTIR spectrum of Tl-bearing voltaite (Fig. 7a) shows strong and broad absorption bands in the range 3900–2900 cm^{-1}, related to the O–H stretching modes of H_2O groups centered around 3573, 3448, 3250, and 3102 cm^{-1}. Two distinctive bands at 1688 and 1638 cm^{-1} can be attributed to the bending of H_2O groups. Applying the relation of Libowitzky (1999), the following distances can be calculated (in Å): 2.67, 2.72, 2.84, and 3.10 Å. Indeed, the short O(3)···Ow(6) are likely the result of the average position of Ow(6), affecting the actual position of O(3), as indicated by the relatively high U_{eq} value, the highest among O atoms in voltaite, in agreement with Mereiter (1972).

Since all H_2O groups are bonded to K, Al, or *M* sites, the chemical formula of voltaite should be correctly written as $K_2Fe^{2+}_5Fe^{3+}_3Al(SO_4)_{12}(H_2O)_{18}$.

Implications

Sulfate mineral assemblages play an important role in the storage and transport of acids and potentially toxic and bioavailable metals released during the weathering of ore deposits, coals, and mine wastes (Jambor et al. 2000). Therefore, as stressed by several authors (e.g., Jamieson 2011; Nordstrom 2011), the characterization of the mineralogy and geochemistry of oxidation products is crucial for predicting their environmental impact and the solid-phase controls on dissolved metal concentration. This characterization involves the accurate knowledge of the crystal-chemistry of sulfate minerals, a goal that can be achieved only through a multi-technique approach, integrating chemical, structural, and spectroscopic data.

Thallium can occur in minor to trace amounts in several ore deposits and can represent a potential environmental hazard (e.g., Xiao et al. 2004). However, this element can be overlooked, and its occurrence could be revealed, for instance, through the accurate study of secondary mineral assemblages. Previous geochemical studies (e.g., Vlasov 1966) highlighted a complex behavior shown by Tl in the oxidation zone that can be summarized in four stages.

(1) Thallium is usually removed, and it does not appear in the common sulfates forming during the earliest stages of sulfides oxidation. Taking into account pyrite oxidation, this stage may correspond to the crystallization of Fe^{2+} and mixed Fe^{2+}/Fe^{3+} species (e.g., Jambor et al. 2000).

(2) The content of thallium can increase following the crystallization of alunite group minerals (e.g., jarosite). This stage corresponds to the latest stage of sulfate crystallization, preceding the formation of iron oxy-hydroxides (e.g., Jambor et al. 2000).

(3) When iron oxy-hydroxides are formed, thallium-bearing

species are usually dissolved and removed again.

(4) Finally, thallium can be oxidized from Tl^{+} to Tl^{3+}, forming the virtually insoluble mineral avicennite.

The mineralogy of thallium in secondary environments in limited to very few species. Avicennite, Tl_2O_3 (Karpova et al. 1958; Radtke et al. 1978), is the only known Tl^{3+} oxide and it is usually found in deeply altered occurrences (e.g., Buus, Switzerland; Herrmann et al. 2018). As reported in the introduction, the three Tl^{+}-oxysalts dorallcharite (Balić-Žunić et al. 1994), lanmuchangite (Chen and Wang 2001), and thalliumpharmacosiderite (Rumsey et al. 2014) are the other known species. Dorallcharite is the Tl-analog of jarosite and crystallizes during stage 2. On the contrary, lanmuchangite is associated, at its type locality, with melanterite, pickeringite, alum-(K), jarosite, and gypsum (Chen and Wang 2001), and it belongs to stage 1. No information about the occurrence of thalliumpharmacosiderite (Rumsey et al. 2014) is available, as the publication is still pending. However, bariopharmacosiderite was observed in the deeply oxidized assemblage of Buus (Herrmann et al. 2018) and likely its thallium-analog could be a mineral formed during the latest stages of ore weathering. In addition, it is well known that Tl^{+} can occur in soils, being hosted in micaceous phyllosilicates (e.g., illite; Herrmann et al. 2018), and can occur as Tl^{+} or Tl^{3+} in Mn oxides. Likely, this could be the genesis of the recently approved mineral thalliomelane, $TlMn^{4+}_{7.5}Cu^{2+}_{0.5}O_{16}$ (Gołębiowska et al. 2020).

The description of thallium-bearing sulfates from the Fornovolasco mining complex, representing an early assemblage in the oxidation of Tl-bearing pyrite ores, suggests that thallium can be transiently sequestered by potassium sulfates during the first stages of weathering, promoting its change of speciation, from a trace element in pyrite ores (up to 1110 μg/g; D'Orazio et al. 2017) to a major constituent of secondary assemblages, achieving concentrations up to some weight unit percent. This behavior disagrees with the description given above (Vlasov 1966). In our opinion, this disagreement could be due the occurrence of K-rich phases in the early stages of oxidation, that could promote the thallium concentration in crystallizing sulfates; in other K-poor environments, where alum-(K) and voltaite do not crystallize, it is very likely that the thallium behavior may follow the behavior described by Vlasov (1966). In addition, it seems likely that the Tl-enrichment occurs late during the first stage of oxidation. The present study, as well as previous contributions (e.g., Kovács-Pálffy et al. 2011), suggests that Tl is enriched during the final stages of the crystal growth of Tl-bearing sulfates, as exemplified by the Tl-enriched rims of voltaite. This could have an environmental significance, as the partial dissolution of voltaite crystals may be sufficient to release high amounts of Tl in water since this element is more concentrated in the outer rims of the crystals.

The occurrence of thallium is usually neglected, and this could also be due to analytical difficulties. For instance, a routinary EDS analysis may fail to detect the occurrence of minor Tl, owing to the interference between Tl*M*α and S*K*α lines. This study shows that, in the case of alum-(K), Raman spectroscopy could reveal the substitution of K^{+} by larger cations; if FTIR spectroscopy does not reveal the occurrence of N–H vibrational modes, then Tl could be a good candidate for being the K-substituent.

As alum-(K) and voltaite are among the more common K-bearing minerals in sulfate assemblages occurring in weathered pyrite ore deposits, their crystal chemistry can dramatically influence the composition of water draining from these areas. Indeed, they could play a central role in storing and temporarily sequestering Tl, acting as scavengers of this element in acid mine drainage systems. During dry conditions, Tl is sequestered and hosted in the crystal structure of these potassium sulfates. On the contrary, during the wet season or flood events, sulfate assemblages can be partially or totally dissolved, contributing pulses of potentially bioavailable metals and metalloids (among which Tl) in the hydrosphere. Consequently, a good knowledge of the crystal chemistry of alum-(K) and voltaite gives additional useful information to understand the processes related to acid mine drainage systems.

Acknowledgments

XAS measurements were performed during experiment 08-01-1016 and in-house beamtime, Francesco d'Acapito and LISA staff members are thanked for the provision of the beamtime. The paper benefited of the constructive comments by Igor Pekov and two anonymous reviewers.

Funding

This research received support from the Ministero dell'Istruzione, dell'Università e della Ricerca through the projects SIR 2014 "THALMIGEN—Thallium: Mineralogy, Geochemistry, and Environmental Hazards" (Grant No. RBSI14A1CV) and from the University of Pisa through the project P.R.A. 2018–2019 "Georisorse e Ambiente" (Grant No. PRA_2018_41). The University Centrum for Applied Geosciences (UCAG) is thanked for the access to the Eugen F. Stumpfl electron microprobe laboratory of Leoben (Austria).

References cited

Ankudinov, A.L., Ravel, B., Rehr, J.J., and Conradson, S.D. (1998) Real-space multiple-scattering calculation and interpretation of X-ray absorption near-edge structure. Physical Review B, 58, 7565–7576.

Balić-Žunić, T., Moëlo, Y., Lončar, Z., and Micheelsen, H. (1994) Dorallcharite, $Tl_{0.8}K_{0.2}Fe_3(SO_4)_2(OH)_6$, a new member of the jarosite-alunite family. European Journal of Mineralogy, 6, 255–263.

Ballirano, P. (2015) Thermal behaviour of alum-(K) $KAl(SO_4)_2 \cdot 12H_2O$ from in situ laboratory high-temperature powder X-ray diffraction data: thermal expansion and modelling of the sulfate orientational disorder. Mineralogical Magazine, 79, 157–170.

Beevers, C.A., and Lipson, H. (1934) Crystal structure of the alums. Nature, 134, 327.

Biagioni, C., Bonaccorsi, E., and Orlandi, P. (2011) Volaschioite, $Fe^{3+}_4(SO_4)O_2(OH)_6 \cdot 2H_2O$, a new mineral species from Fornovolasco, Apuan Alps, Tuscany, Italy. Canadian Mineralogist, 49, 605–614.

Biagioni, C., D'Orazio, M., Vezzoni, S., Dini, A., and Orlandi, P. (2013) Mobilization of Tl-Hg-As-Sb-(Ag,Cu)-Pb sulfosalt melts during low-grade metamorphism in the Alpi Apuane (Tuscany, Italy). Geology, 41, 747–750.

Biagioni, C., D'Orazio, M., Lepore, G.O., d'Acapito, F., and Vezzoni, S. (2017) Thallium-rich rust scales in drinkable water distribution systems: A case study from northern Tuscany, Italy. Science of the Total Environment, 587-588, 491–501.

Brese, N.E., and O'Keeffe, M. (1991) Bond-valence parameters for anion-anion bonds in solids. Acta Crystallographica, B48, 152–154.

Bruker AXS Inc. (2004) APEX 2. Bruker Advanced X-ray Solutions, Madison, Wisconsin, U.S.A.

Chen, D., and Wang, G. (2001) A new mineral—lanmuchangite. Acta Mineralogica Sinica, 21, 271–277.

Cordsen, A. (1978) A crystal-structure refinement of libethenite. Canadian Mineralogist, 16, 153–157.

Cork, J.M. (1927) The crystal structure of some of the alums. Philosophical Magazine, 4, 688–698.

Craw, D. (1981) Oxidation and microprobe-induced potassium mobility in iron-bearing phyllosilicates from the Otago schists, New Zealand. Lithos, 14, 49–57.

d'Acapito, F., Trapananti, A., Torrengo, S., and Mobilio, S. (2014) X-ray absorption spectroscopy: The Italian beamline GILDA at the ESRF. Notiziario Neutroni e Luce di Sincrotrone, 19, 14.

d'Acapito, F., Lepore, G.O., Puri, A., Laloni, A., La Manna, F., Dettona, E., De Luisa, A., and Martin, A. (2019) The LISA beamline at ESRF. Journal of Synchrotron Radiation, 26, 551–558.

D'Orazio, M., Biagioni, C., Dini, A., and Vezzoni, S. (2017) Thallium-rich pyrite ores from the Apuan Alps, Tuscany, Italy: Constraints for their origin and environmental concerns. Mineralium Deposita, 52, 687–707.

Dyar, M.D., Jawin, E.R. and Sklute, E. (2013) Mössbauer parameters of iron sulfate minerals. American Mineralogist, 98, 1943–1965.

Ertl, A., Dyar, M.D., Hughes, J.M., Brandstätter, F., Gunter, M.E., Prem, M., and Peterson, R.C. (2008) Pertlikite, a new tetragonal Mg-rich member of the voltaite group from

Madeni Zakh, Iran. Canadian Mineralogist, 46, 661–669.
Ferraris, G., and Franchini-Angela, M. (1972) Survey of the geometry and environment of water molecules in crystalline hydrates studied by neutron diffraction. Acta Crystallographica, B28, 3572–3583.
Ferraris, G., and Ivaldi, G. (1988) Bond valence vs bond length in O···O hydrogen bonds. Acta Crystallographica, B44, 341–344.
Frost, R.L., and Kloprogge, J.T. (2001) Raman microscopy study of kalinite, tschermigite and lonecreekite at 298 and 77 K. Neues Jahrbuch für Mineralogie Monatshefte, 2001, 27–40.
George, L.L., Biagioni, C., D'Orazio, M., and Cook, N.J. (2018) Textural and trace element evolution of pyrite during greenschist facies metamorphic recrystallization in the southern Apuan Alps (Tuscany, Italy): Influence on the formation of Tl-rich sulfosalt melt. Ore Geology Reviews, 102, 59–105.
Ghezzi, L., D'Orazio, M., Doveri, M., Lelli, M., Petrini, R., and Giannecchini, R. (2019) Groundwater and potentially toxic elements in a dismissed mining area: Thallium contamination of drinking spring water in the Apuan Alps (Tuscany, Italy). Journal of Geochemical Exploration, 197, 84–92.
Gołębiowska, B., Pieczka, A., Zubko, M., Voegelin, A., Göttlicher, J., and Rzepa, G. (2020) Thalliomelane, IMA 2019-055. CNMNC Newsletter No. 52, European Journal of Mineralogy, 32, 1–11
Gossner, B., and Besslein, J. (1934) Hydrated sulfates of three metals. Centralblatt für Mineralogie, Geologie, und Paläontologie 1934A, 358–364 (in German).
Gossner, B., and Drexler, K. (1933) Structural and molecular units of sulfates of the voltaite type. Centralblatt für Mineralogie, Geologie, und Paläontologie 1933A, 83–91 (in German).
Gossner, B., and Fell, E. (1932) Beitrag zur Kenntnis voltait-artiger Sulfate. Berichte der deutschen chemischen Gesellschaft, 65B, 393–395.
Götz, A., Mihalka, St., Ionita, I., and Toth, Z. (1968) Monsmeditul—un nuo mineral de taliu de la Baia Sprie. Revista Mineralor, 19, 154–159.
Grice, J.D., and Ferraris, G. (2003) New minerals approved in 2002 and nomenclature modifications approved in 1998–2002 by the Commission on New Minerals and Mineral Names, International Mineralogical Association. Canadian Mineralogist, 41, 795–802.
Hawthorne, F.C., Krivovichev, S.V., and Burns, P.C. (2000) The crystal chemistry of sulfate minerals. Reviews in Mineralogy and Geochemistry, 40, 1–101.
Herrmann, J., Voegelin, A., Palatinus, L., Mangold, S., and Majzlan, J. (2018) Secondary Fe-As-Tl mineralization in soils near Buus in the Swiss Jura Mountains. European Journal of Mineralogy, 30, 887–898.
Jambor, J.L., Nordstrom, D.K., and Alpers, C.N. (2000) Metal-sulfate salts from sulfide mineral oxidation. Reviews in Mineralogy and Geochemistry, 40, 303–350.
Jamieson, H.E. (2011) Geochemistry and mineralogy of solid mine waste: essential knowledge for predicting environmental impact. Elements, 7, 381–386.
Johan, Z., Udubasa, G., and Zemann, J. (2009) "Monsmedite", a discredited potassium thallium sulphate mineral from Baia Sprie and its identity with voltaite: The state of the art. Neues Jahrbuch für Mineralogie Abhandlungen, 186, 63–66.
Karpova, K.N., Kon'kova, E.A., Larkin, E.D., and Savel'ev, V.F. (1958) Avicennite—a new mineral. Doklady Akademii Nauk Uzbekskoi SSR, 2, 23–26 (in Russian).
Keith, L.H., and Telliard, W.A. (1979) Priority pollutants: I-a perspective view. Environmental Science and Technology, 13, 416–423.
Košek, F., Edwards, H.G.M., and Jehlička, J. (2019) Raman spectroscopic vibrational analysis of the complex iron sulfates clairite, metavoltine, and voltaite from the burning coal dump Anna I, Alsdorf, Germany. Journal of Raman Spectroscopy, 1–8.
Kovács-Pálffy, P., Muske, J., Földvári, M., Kónya, P., Homonnay, Z., Ntaflos, T., Papp, G., Király, E., Sajó, I., Szilágyi, V., and Boszó, G. (2011) Detailed study of "monsmedite" specimens from the original (1963) find, Baia Sprie, Baia Mare Ore District (Romania). Carpathian Journal of Earth and Environmental Sciences, 6, 321–330.
Larson, A.C., and Cromer, D.T. (1967) Refinement of the alum structures. III. X-ray study of the α alums, K, Rb and $NH_4Al(SO_4)_2 \cdot 12H_2O$. Acta Crystallographica, 22, 793–800.
Lee, P.A., Citrin, P.H., Eisenberger, P.T., and Kincaid, B.M. (1981) Extended X-ray absorption fine structure—its strengths and limitations as a structural tool. Reviews of Modern Physics, 53, 769–806.
Libowitzky, E. (1999) Correlation of O–H stretching frequencies and O–H···O hydrogen bond lengths in minerals. Monatshefte für Chemie, 130, 1047–1059.
Lipson, H. (1935) The relation between the alum structures. Proceedings of the Royal Society of London, Series A, Mathematical and Physical Sciences, 151, 347–356.
Kampf, A.R., Richards, R.P., Nash, B.P., Murowchick, J.B., and Rakovan, J.F. (2016) Carlsonite, $(NH_4)_5Fe^{3+}O(SO_4)_6 \cdot 7H_2O$, and huizingite-(Al), $(NH_4)_9Al_3(SO_4)_8(OH)_2 \cdot 4H_2O$, two new minerals from a natural fire in an oil-bearing shale near Milan, Ohio. American Mineralogist, 101, 2095–2107.
Majzlan, J., Schlicht, H., Wierzbicka-Wieczorek, M., Giester, G., Pöllmann, H., Brömme, B., Doyle, S., Buth, G., and Koch, C.B. (2013) A contribution to the crystal chemistry of the voltaite group: solid solutions, Mössbauer and infrared spectra, and anomalous anisotropy. Mineralogy and Petrology, 107, 221–233.
Manilici, V., Giusca, D., and Stiopol, V. (1965) Studiul zacamintului de la Baia Sprie (Reg. Baia Mare). Memoriile Comitetului Geologic, 7, 1–113.
Martini, J.E.J. (1983) Lonecreekite, sabieite and clairite, new secondary ammonium ferric iron sulphates from Lone Creek Fall Cave, near Sabie, eastern Transvaal. Annals of the Geological Survey of South Africa, 17, 29–34.
Mereiter, K. (1972) Die Kristallstruktur des Voltaits, $K_2Fe^{2+}_5Fe^{3+}_3Al[SO_4]_{12} \cdot 18H_2O$, Tschermaks Mineralogische und Petrographische Mitteilungen, 18, 185–202.
Nordstrom, D.K. (2011) Mine waters: acidic to circumneutral. Elements, 7, 393–398.
Nyburg, S.C., Steed, J.W., Aleksovska, S., and Petruševski, V.M. (2000) Structure of the alums. I. On the sulfate group disorder in the α-alums. Acta Crystallographica, B56, 204–209.
Perotti, M., Petrini, R., D'Orazio, M., Ghezzi, L., Giannecchini, R., and Vezzoni, S. (2018) Thallium and other potentially toxic elements in the Baccatoio stream catchment (Northern Tuscany, Italy) receiving drainages from abandoned mines. Mine Water Environment, 37, 431–441.
Prescher, C., McCammon, C., and Dubrovinsky, L. (2012) MossA: a program for analyzing energy-domain Mössbauer spectra from conventional and synchrotron sources. Journal of Applied Crystallography, 45, 329–331.
Puri, A., Lepore, G.O., and d'Acapito, F. (2019) The New Beamline LISA at ESRF: Performances and Perspectives for Earth and Environmental Sciences. Condensed Matter, 4, 12.
Radtke, A.S., Dickson, F.W., and Slack, J.F. (1978) Occurrence and formation of avicennite, Tl_2O_3, as a secondary mineral at the Carlin gold deposit, Nevada. Journal of Research USGS, 6, 241–246.
Ravel, B. (2001) ATOMS: Crystallography for the X-ray absorption spectroscopist. Journal of Synchrotron Radiation, 8, 314–316.
Ravel, B., and Newville, M. (2005) ATHENA, ARTEMIS, HEPHAESTUS: data analysis for X-ray absorption spectroscopy using IFEFFIT. Journal of Synchrotron Radiation, 12, 537–541.
Roberts, A.C., Venance, K.E., Seward, T.M., Grice, J.D., and Paar, W.H. (2006) Lafossaite, a new mineral from the La Fossa crater, Vulcano, Italy. Mineralogical Magazine, 37, 165–168.
Rumsey, M.S., Mills, S.J., Spratt, J., Hay, D.G., and Farber, G. (2014) Thalliumpharmacosiderite, IMA 2013-124. CNMNC Newsletter No. 20, June 2014, p. 553; Mineralogical Magazine, 78, 549–558.
Schwarte, C., and Fischer, W. (1989) Zur Kristallstruktur des K-Mg-Fe-Voltaits. Zeitschrift für Kristallographie, 186, 272–273.
Shannon, R.D. (1976) Revised effective ionic radii and systematic studies of interatomic distances in halides and chalcogenides. Acta Crystallographica, A32, 751–767.
Sheldrick, G.M. (2015) Crystal structure refinement with SHELXL. Acta Crystallographica, C71, 3–8.
Szakáll, S., Sajó, I., Fehér, B., and Bigi, S. (2012) Ammoniomagnesiovoltaite, a new voltaite-related mineral species from Pécs-Vasas, Hungary. Canadian Mineralogist, 50, 65–72.
van der Pluijm, B., Lee, J.H., and Peacor, D.R. (1988) Analytical electron microscopy and the problem of potassium diffusion. Clays and Clay Minerals, 36, 498–504.
Vlasov, K.A. (Ed.) (1966) Geochemistry and mineralogy of rare elements and genetic types of their deposits. Geochemistry of Rare Elements, vol. 1, p. 491–524. Israel Program for Scientific Translations.
Wedepohl, K.H. (1995) The composition of the continental crust. Geochimica et Cosmochimica Acta, 59, 1217–1239.
Williams, P.A., Leverett, P., Birch, W.D., Hibbs, D.E., Kolitsch, U., and Mihajlovic, T. (2006) Zinc-rich zincolibethenite from Broken Hill, New South Wales. Australian Journal of Mineralogy, 12, 3–7.
Wilson, A.J.C. (1992) International Tables for Crystallography Volume C. Kluwer, Dordrecht.
Wojdyr, M. (2010) Fityk: a general-purpose peak fitting program. Journal of Applied Crystallography, 43, 1126–1128.
Xiao, T., Guha, J., Boyle, D., Liu, C.-Q., Zheng, B., Wilson, G.C., Rouleau, A., and Chen, J. (2004) Naturally occurring thallium: a hidden geoenvironmental health hazard? Environment International, 30, 501–507.
Zemann, J. (1993) What is monsmedite? Romanian Journal of Mineralogy, 76, 97–98.
Zhitova, E.S., Siidra, O.I., Belakovsky, D.I., Shilovskikh, V.V., Nuzhdaev, A.A., and Ismagilova, R.M. (2018) Ammoniovoltaite, $(NH_4)_2Fe^{2+}_5Fe^{3+}_3Al(SO_4)_{12}(H_2O)_{18}$, a new mineral from the Severo-Kambalny geothermal field, Kamchatka, Russia. Mineralogical Magazine, 82, 1057–1077.
Zhitova, E.S., Sergeeva, A.V., Nuzhdaev, A.A., Krzhizhanovskaya, M.G., and Chubarov, V.M. (2019) Tschermigite from thermal fields of southern Kamchatka: high-temperature transformation and peculiarities of IR-spectrum. Proceedings of the Russian Mineralogical Society, 148, 100–116.

Manuscript received October 10, 2019
Manuscript accepted February 2, 2020
Manuscript handled by Paolo Lotti

Endnote:

[1]Deposit item AM-20-77320, Supplemental Figure and CIF. Deposit items are free to all readers and found on the MSA website, via the specific issue's Table of Contents (go to http://www.minsocam.org/MSA/AmMin/TOC/2020/Jul2020_data/Jul2020_data.html).